Exciton dynamics in two-dimensional MoS_{2} on a hyperbolic metamaterial-based nanophotonic platform

Kwang Jin Lee, Wei Xin, Chunhao Fann, Xinli Ma, Fei Xing, Jing Liu, Jihua Zhang, Mohamed Elkabbash, and Chunlei Guo

Phys. Rev. B **101**, 041405 — Published 13 January 2020

DOI: 10.1103/PhysRevB.101.041405

Exciton dynamics in two-dimensional MoS_2 on hyperbolic metamaterial-based nanophotonic platform

Kwang Jin Lee[1], Wei Xin[2], Chunhao Fann[1], Xinli Ma[3], Fei Xing[4], Jing Liu[3], Jihua Zhang[1], Mohamed Elkabbash[1], Chunlei Guo[1]*

[1] Institute of Optics, University of Rochester, Rochester, New York, USA,

[2] GPL, Changchun Institute of Optics, Fine Mechanics and Physics, Chinese Academy of Sciences, Changchun, China, 130033

[3]State Key Laboratory of Precision Measurement Technology and Instruments, School of Precision Instruments and Opto-electronics Engineering, Tianjin University, Tianjin, China, 300072

[4]School of Physics and Optoelectronic Engineering, Shandong University of Technology, Zibo, China, 255049

*Correspondence author E-mail: guo@optics.rochester.edu

The discovery of two-dimensional transition metal dichalcogenides (2D TMDs) has promised next-generation photonics and optoelectronics applications, particularly in the realm of nanophotonics. Arguably, the most crucial fundamental processes in these applications are the exciton migration and charge transfer in 2D TMDs. However, exciton dynamics in 2D TMDs have never been studied on a nanophotonic platform and more importantly, the control of exciton dynamics by means of nanophotonic structures has yet to be explored. Here, for the first time, we demonstrate the control of exciton dynamics in MoS_2 monolayers by introducing a hyperbolic metamaterial (HMM) substrate. We reveal the migration mechanisms of various excitons in MoS_2 monolayers. Furthermore, we experimentally demonstrate that the Förster radius can be increased by HMMs, which is completely

consistent with the theory we developed on the basis of nonlocal effects of HMM. This study will provide a significant step forward in enabling 2D TMD nanophotonics hybrid devices.

With the explosive research activities since the discovery of graphene, two-dimensional (2D) materials have emerged as one of the most exciting areas studied in science and engineering[1-5]. Among them, 2D transition metal dichalcogenides (TMDs) have attracted a great amount of attentions and been considered as an ideal material for nanophotonic and optoelectronic applications due to their remarkable optical and electronic properties, such as, higher photo-luminescence efficiency due to direct bandgap and existence of light-valley interactions[6-11]. Atomically-thin monolayer TMDs have strongly bounded excitons because of the enhancement in quantum confinement and Coulomb interactions, and this strong bonding dominates most optical and electronic effects. In general, exciton binding energy in TMD monolayers is an order of magnitude higher than that of previously investigated 2D quantum well structures, which leads to their unique optoelectronic characteristics and makes TMDs an ideal platform for exploring exciton dynamics (ED) that is essential for photo-current conversion processes and novel optoelectronic applications[12,13]. An analogue can be seen in organic semiconductors, which also have large exciton binding energies due to their low dielectric constants and this effect incites a large amount of exciton dynamics studies in organic photovoltaic operation [14-17]. Therefore, a thorough characterization of ED is of paramount importance for improving light-harvesting applications as well as revealing fundamental mechanism of carrier dynamics in 2D TMDs. More importantly, controlling the ED in these materials is crucial in developing novel optoelectronic devices. Although various excitonic properties including ED, exciton lifetime, and exciton band structures in 2D TMDs alone have been intensively studied in recent years [18-21], the control of ED in 2D TMDs by using nanophotonic structure has never been explored before.

Engineering light-matter interactions has been realized using nanophotonic structures, e.g., metamaterials and engineered materials with tailored optical properties [22-24]. Particularly, metamaterials have been used in optoelectronic devices [25,26], optical sensing [27], plasmonic lasers [28] and Raman spectroscopy [29]. Among various types of metamaterials, hyperbolic metamaterials (HMMs) have been extensively studied over the past few years due to their unusual optical properties from the high-*k* states [30-34]. HMM structures that have been shown to exert nonlocal effects on the photophysical properties of their surrounding environment have recently been reported [35,36], which suggests that the optical property of 2D TMDs can be drastically altered without modifying the material itself, but instead by incorporating them on a HMM.

MoS_2 monolayers exhibit two typical band-edge excitons, A- and B-excitons, resulting from transitions between the conduction band minimum and spin-orbit split valence band maximum near the K point. In addition, recent studies observed another exciton, labelled as C-excitons, with a strong and broadband absorption at higher energies. C-exciton states are attributed to the band nesting effect, i.e., transition arising from the maxima in the joint density of state when the conduction and valence bands are parallel in a region between *K* and *Γ* points [37-41]. Unlike A- and B-excitons, C-excitons have no photoluminescence. Although several studies have attempted to address some aspects of ED in 2D TMDs [42-45], the exact mechanism of exciton migration dynamics still remains unclear. Therefore, there has been no study on controlling the exciton migration process of these materials.

In this letter, we comprehensively study the underlying mechanisms of exciton migration dynamics in 2D MoS_2 and its controllability based on the HMM-based nanophotonic platform. We demonstrate that ED in the A- and C-excitons show very different dynamic process; the migration of A-exciton is mainly through a single-step Förster-type resonance energy transfer (FRET)

whereas multi-step diffusion process is responsible for C-excitons. We also find that the Förster radius increases in the presence of the HMM substrates in the hyperbolic dispersion region, but the diffusion coefficient is not affected by the HMMs. We elucidate that the increased Förster radius comes from the nonlocal effects of HMMs from the Purcell effect. We note there has been ongoing debates in understanding FRET in complex photonic environment [46], and this study provides conclusive evidence to address these issues.

MoS_2 monolayer was prepared on silicon substrates by means of chemical vapor deposition. Single-layer samples were identified by optical microscopy and photoluminescence map shown in Figure S1 [47]. Multi-layered HMMs consisting of 5 pairs of alternative Ag-TiO_2 layers with different fill factors (f = 0.2, 0.5, and 0.8) were fabricated by electron beam evaporation. Detailed sample configurations are described in Figure S2 [47]. We confirmed that the peaks of Raman spectra were not altered with HMM substrates (Supplementary material - Figure S3). In our design, a 10-nm thick Al_2O_3 layer was deposited on top of the stack to avoid the convolution of other processes such as charge transport between MoS_2 and HMMs (Supplementary material - Figure S4). Figure 1a schematically displays the sample configuration for MoS_2 monolayer deposited on a HMM substrate with f = 0.5 (10 nm thickness of each layer). To observe the ED, we used exciton-exciton annihilation (EEA) method by performing ultrafast transient absorption (TA) experiment based on the pump-probe technique described below. Figure 1b shows the absorption and photoluminescence spectra of MoS_2 monolayer. The two absorption peaks at 1.87 eV and 2.05 eV correspond to A- and B-excitons of MoS_2 monolayers, respectively. The broad absorption band above 2.80 eV corresponds to the non-emissive C-excitons. The photoluminescence peak and shoulder at 1.84 eV and 2.01 eV correspond to A- and B-excitons, respectively. Figure 1c presents the real part of an effective dielectric constant of HMMs along the transverse direction calculated

by effective medium theory. HMM with $f = 0.8$ ($f = 0.2$) shows hyperbolic (elliptic) dispersions region for both A-and C-excitons, whereas HMM with $f = 0.5$ exhibits hyperbolic (elliptic) dispersion for A- (C-) excitons.

Ultrafast TA experiments were carried out to analyze the ED of MoS_2 monolayers by measuring relative reflection ($\Delta R/R$). The pump beam at 2.25 eV (3.05 eV) and probe beam at 1.85 eV (3.05 eV) were chosen for A- (C-) excitons. The pump fluence for A- and C-excitons were adjusted to obtain the same initial exciton densities (n_0) immediately after the excitation by the pump. We note that TA signal of Si is negligible compared to the TA signal of 2D MoS_2 at the frequency range of interest. This allows us to obtain the pure TA signal of MoS_2 by subtracting TA signal of Si substrate from the entire TA signal. (Supplementary material - Figure S5) Figures 2a and 2b show the normalized TA kinetics of A- and C-excitons in MoS_2 monolayer on Si substrate without metamaterials for different exciton densities. At the lowest initial exciton density (n_0=0.06 × 10^{12} cm^{-2}), TA kinetics for both A- and C-excitons are fitted by a mono-exponential decay functions with characteristic time (τ) of about 186 ps and 213 ps, corresponding to the intrinsic exciton lifetimes. C-excitons have a relatively longer lifetime than A-excitons, and this is consistent with previous works showing that favorable band alignment and transient excited state Coulomb environment could lead to a longer lifetime of C-excitons [37,40]. The lifetime of A-excitons based on TA measurement (τ = 186 ps) is similar to emission lifetime obtained by time-resolved photoluminescence measurement (τ_{PL} = 175 ps) as shown in Figure S6 [47]. As n_0 increases, the decay of A-excitons deviates from a mono-exponential fitting due to an EEA taking place where two excitons are sufficiently close to interact and to generate a single exciton with a higher energy. Using bi-exponential decay fitting, we found that the short time constant (τ_1) decreases with n_0. On the other hand, the longer time constant (τ_2) is almost independent of n_0, indicating that τ_1

represents EEA phenomenon and τ_2 corresponds to the intrinsic exciton lifetime (Supplementary material - Figure S7). For C-exciton, we observed a relatively weak dependence on n_0, which is also consistent with previous work suggesting that the exciton dissociation occurs efficiently, in agreement with the self-separation of photocarriers in the nesting region in the momentum space [41]. In addition, for A-excitons, we note that figure 2a is consistent with previous study [42].

Figures 2c and 2d display the TA decays for A- and C-excitons in the initial time range (up to ~ 100 ps). To analyze the EEA behavior, we consider the rate equation of EEA described by [48,49]

$$\frac{d}{dt}n(t) = -\frac{n(t)}{\tau} - \frac{1}{2}\gamma(t)n(t)^2 \quad (1)$$

where $n(t)$ is the exciton density at a delay time t after the excitation, $\gamma(t)$ is the annihilation rate coefficient and τ is intrinsic the exciton lifetime at the low exciton density limit (τ_2). The factor 1/2 represents that only one exciton is left after EEA. We note that EEA is dominant over the Auger recombination in this structure [39]. In general, EEA process can be classified as two different mechanisms: multi-step exciton diffusions and a single-step FRET [48,49]. The exciton diffusion model assumes that the excitons move in random walk in many steps towards each other before the annihilation takes place. On the other hand, FRET model considers that annihilation occurs directly via long-range energy transfer processes. FRET strongly depends on the overlap between the emission spectrum of the donor and the absorption spectrum of the acceptor. Here, the FRET process between two identical excitons can depend on a spectral overlap between the exciton emission and the excited state absorption, which is the absorption from the first exciton state to higher electronic states.

For MoS_2 monolayers, we only need to consider FRET and 1D exciton diffusion mechanisms. $\gamma(t)$ is given by $\alpha \cdot t^{-1/2}$ where $\alpha = R_F^2 \pi^{3/2} / 2\tau^{1/2}$ for the FRET model with R_F is the Förster radius and

$\alpha=(8D/\pi)^{1/2}/aN_0$ for the 1D diffusion model with the diffusion coefficient D, lattice constant a and molecular density N_0. From these relations, Eq. (1) can be solved as [48,49],

$$n(t)=\frac{n_0 e^{-t/\tau}}{1+\beta\,\mathrm{erf}\left(\sqrt{\frac{t}{\tau}}\right)} \tag{2}$$

where 'erf' is the error function. The coefficient β is expressed by $n_0R_F^2\pi^2/4$ and n_0l_D/aN_0 for FRET and the 1D diffusion process, respectively. l_D is the diffusion length defined as $(2D\tau)^{1/2}$. (Supplementary material-section II) The a and N_0 of MoS_2 monolayers were taken as 3.16 Å and 5.7×10^{14} cm^{-2}, respectively. Here, it is worth noting that $n(t)$ for both the FRET and 1D exciton diffusion models have the same mathematical structure. We have also considered 2D and 3D exciton diffusion models and fit the experimental results of C-exciton density kinetics with the 2D model. Figure S8 [47] shows that the best fit was obtained using the 1D exciton diffusion model, indicating that the diffusion coefficient of C-excitons is strongly anisotropic and thus allows effective diffusion only along one dimension in a 2D MoS_2. (Supplemental material-section III, see, also, references [51] therein)

The solid curves in Figures 2b and 2e represent the fits based on Eq. (2). For C-excitons, FRET was excluded due to their non-emissive property [48]. The diffusion coefficient D determined from the fits of the TA decays based on the 1D diffusion model is plotted in Figure 2f. Here, the exciton lifetime τ without annihilation was kept as a constant (τ = 213 ps) and thus was not a fitting parameter.

For A-exciton, the spectral overlap between the emission and the excited state absorption and the decreasing behavior of τ_1 with n_0 (quenching effect of donor exciton) clearly shows that FRET is likely the main mechanism of A-exciton migration. Therefore, we plot the R_F as a function of n_0

for A-exciton in Figure 2e. We find that the value of R_F is around 6.0 ~ 6.4 nm and is hardly dependent on n_0, which is also consistent with the fact that R_F does not depend on the exciton density (Eq. (S8) in the supplementary material).

Figure 3 shows the behavior of time constants with different substrates. We note that τ_1 and τ_2 remain constant for all substrates with no overlapping hyperbolic dispersion, while a discernible decrease in τ_1 and τ_2 is observed for HMM with f=0.5 and 0.8. For A-excitons, the decrease of τ_2 from 186 ps to 150 ps can be easily understood in terms of the Purcell factor enhancement based on the high local density of optical states provided by HMMs. Here, we obtain Purcell factor of ~1.24 from basic relationship given by τ_2^{Si}/τ_2^{HMM}. (Table S1) Interestingly, a shortening of τ_1 due to the hyperbolic dispersion indicates that the nonlocal effect of HMM based on the Purcell factor enhancement clearly affect ED occurring through FRET. The 1p substrate consists of a single pair of 10 nm thick Ag/TiO_2 films with a 10-nm Al_2O_3 serves as a control sample showing the relatively unmodified decay kinetics of MoS_2. For C-excitons, while τ_1 appears to be independent of the substrates, we observed an increase in τ_2 within experimental error. The increase in τ_2 is somewhat similar to the increase in the charge recombination time with the HMM substrates observed in previous studies [35]. The entire TA data were plotted in Figure S9[47]. We note that pump fluence was adjusted to obtain the same n_0 by taking field intensity variation into account in the presence of HMM structure. (Supplementary material - Figure S10)

In Figures 4a and 4b, we plot R_F and D as functions of n_0 for Si and HMM with f=0.2 and 0.8 substrates, respectively. We note that the experimental results for HMM with f=0.5 is almost identical to those for HMM with f=0.8. Figure 4a exhibits an enhancement in R_F for the A-excitons in the HMM hyperbolic dispersion regimes. We can explain this interesting result in terms of the nonlocal effect of HMMs based on the Purcell factor enhancement. It has been shown previously

that the nonlocal effect of HMMs could lead to a decrease in the refractive index of the environment effectively[36]. Here, we can equalize the problem as the emitter is placed in a homogenous medium with modified n. Based on this discussion, we showed that Purcell factor is inversely proportional to n^3. We also apply this concept to FRET, and we obtained the relationship between R_F and Purcell factor (denoted as F_p) as follows, (Supplementary material-section IV).

$$R_{\mathrm{F}} \propto F_p^{\frac{2}{9}} \tag{3}$$

This relation presents a quantitative enhancement factor of R_F by 1.05, which is displayed as the open circles in Figure 4a. Surprisingly, the predicted values based on the nonlocal effect of HMMs are almost consistent with the experimental values. We note that the current MoS_2-HMM hybrid systems are an ideal platform to investigate the fundamental relationship between FRET and photonic environment by excluding quenching effects such as donor-HMM coupling and the charge transport between MoS_2 and HMMs. In case of the diffusion processes, as shown in Figure 4b, there is no noticeable change in the presence of HMMs, which can be explained by the fact that diffusion processes are not relevant for light-matter interactions. Figure 4c schematically illustrates dominant migration mechanisms of A- and C-excitons in 2D MoS_2.

Finally, we discuss the influence of Purcell effect due to HMM on FRET efficiency. We note that FRET efficiency, η_{FRET}, strongly depends on the R_{F} as following equation[50],

$$\eta_{FRET} = \frac{R_{\mathrm{F}}^6}{R_{\mathrm{F}}^6 + r_{\mathrm{T}}^6} = \left[1 + \left(\frac{r_{\mathrm{T}}}{R_{\mathrm{F}}}\right)^6\right]^{-1} \tag{4}$$

where r_{T} is the distance between two molecules. Eq. (4) shows that η_{FRET} is strongly dependent on R_{F} and r_{T}. We calculate the r_{T} for each exciton density, n_0, which are, 5.77 nm, 8.16 nm, 10.54 nm,

18.25 nm for 3.0×10^{12} cm^{-2}, 1.5×10^{12} cm^{-2}, 0.9×10^{12} cm^{-2}, and 0.3×10^{12} cm^{-2}, respectively. On the basis of the values of R_F obtained from the figure 4b, we plot the η_{FRET} as a function of n_0 in Figure 5. We clearly see the ~8.3 % enhancement of η_{FRET} in the presence of HMM for $n_0 = 3.0 \times 10^{12}$ cm^{-2}.

In conclusion, based on the different underlying migration mechanisms of A- and C-exciton dynamics in 2D MoS_2; single-step Förster-type resonance energy transfer for A-exciton and multi-step diffusion process for C-exciton, we investigate the in-depth optical interplay between 2D TMDs and metamaterials by integrating 2D MoS_2 on a range of nanophotonic platforms using HMMs with different fill factors. We find an increase in the Förster radius for A-excitons when A-exciton spectral region lies in the hyperbolic dispersion region. Furthermore, for the first time, we develop a new theoretical model determining the relationship between Förster radius and Purcell factor. Our study clearly shows that HMMs can alter the FRET process. There has been a great amount of controversy if FRET plays a role on the strength of excitation interactions in 2D TMDs in the presence of the surrounding media. We resolve this issue, for the first time, by showing that FRET plays the dominant role in A-exciton. Our work presents a novel way to nano-engineering 2D TMDs with a metamaterial-based nanophotonic platform, which will advance the applications of 2D materials in photonics, optoelectronics, and meta-devices.

Acknowledgments

This research was supported by Bill & Melinda Gates Foundation, National Science Foundation, and National Natural Science Foundation (NSFC, Grant Nos. 11804334).

Author contributions

K.J.L. and W.X. contributed equally to this work.

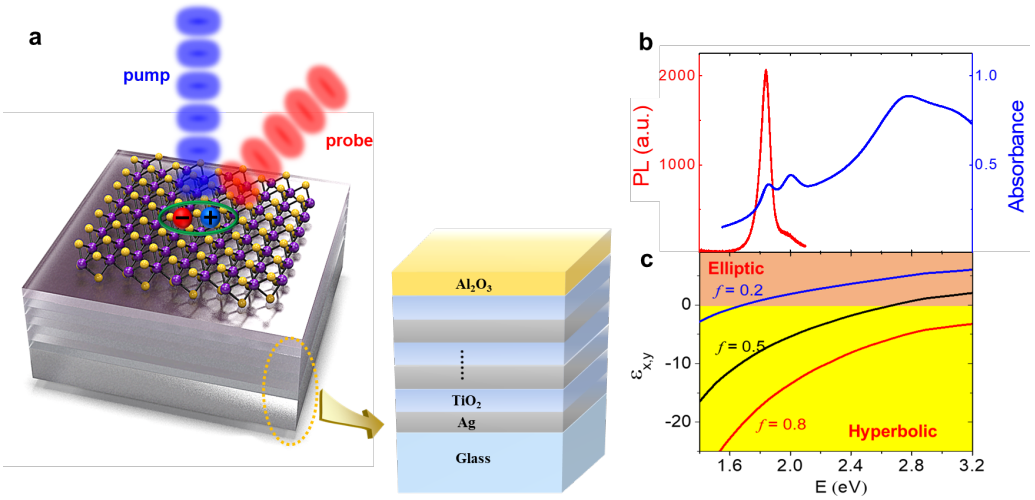

Figure 1. Sample configuration and characterization. a, Schematics of the experimental configuration for a MoS_2 monolayer with exciton dynamics based on the transient absorption measurements. The MoS_2 monolayer is deposited on a multilayered HMM structure that consists of 5 pairs of Ag-TiO_2 layers covered by a Al_2O_3 film to block any charge transport **b,** Absorption and photoluminescence spectra of MoS_2 monolayers with A-,B- and C-excitons. **c,** the Real part of the transverse effective dielectric function of HMM for three different fill factors (f=0.2, 0.5, 0.8)

223

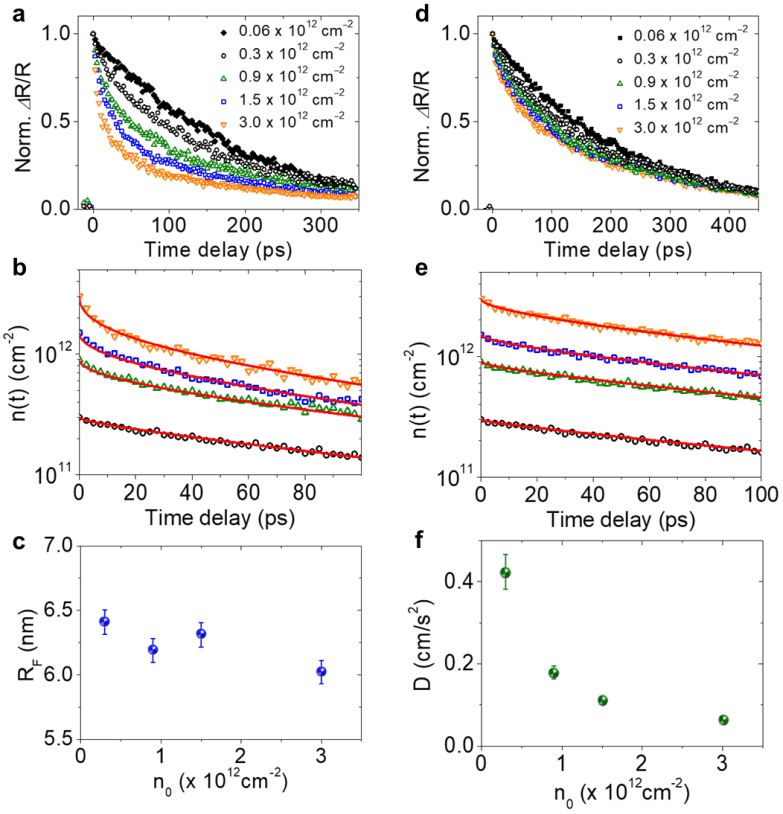

Figure 2. Transient absorption decays and fitting curves based on exciton-exciton annihilation. a~c: A-excitons, **d~f**: C-excitons. a,d, Normalized transient absorption decay of A- and C-excitons respectively for several initial exciton densities. b,e, Exciton decays for A- and C-excitons respectively in the initial time range (up to 100 ps) with fitting curves based on Eq. (2). c, f, the Forster radii and the diffusion coefficients for A- and C-excitons with initial exciton density n_0.

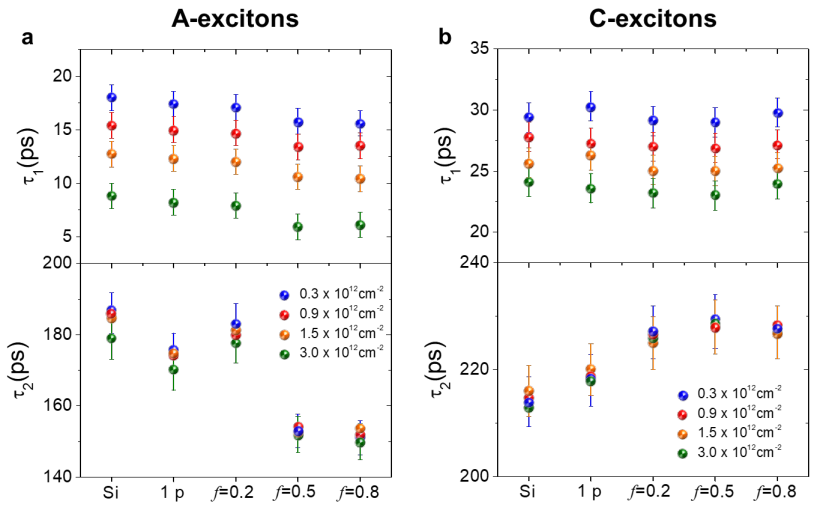

Figure 3. Behaviors of time constants for A- and C-excitons with different substrates a, Short (τ_1) and long (τ_2) characteristic time constants of A-exctions with different substrates for several initial exciton densities. **b,** Short (τ_1) and long (τ_2) characteristic time constants of C-exctions with different substrates for several initial exciton densities.

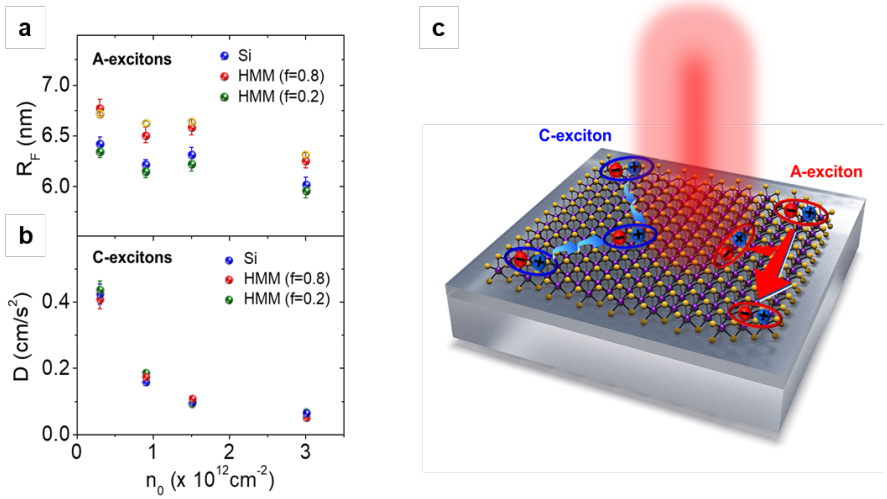

Figure 4. Underlying mechanism for exciton dynamics and behaviors of the Förster radius and diffusion coefficient a, Shematics shows the different migration mechanisms for A- and C-excitons **b,** Förster radius and **c,** the Diffusion coefficients for A- and C-excitons as a function of the initial exciton density on different substrates (Si, HMM with *f*=0.2 and 0.8). The overall measured behaviors for *f*=0.5 are almost identical to those for *f*=0.8.

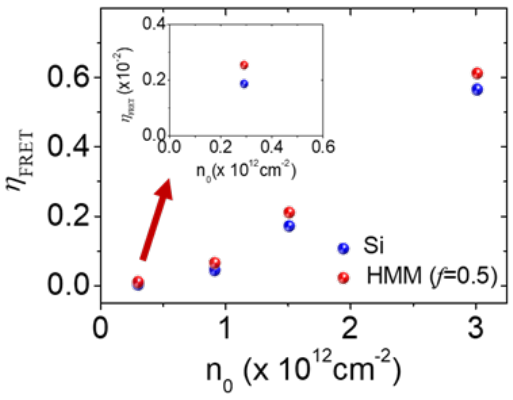

Figure 5. Plot of FRET efficiency versus n_0. FRET efficiency η_{FRET} as a function of n_0 in the absence (blue) and presence (red) of HMM. (inset: magnification at $n_0 = 0.3 \times 10^{12}$ cm^{-2})

References:

[1] A. K. Geim and K. S. Novoselov, The rise of graphene. Nat. Mater. **6**, 183 (2007).

[2] F. Bonaccorso, Z. Sun, T. Hasan, and A. C. Ferrari, Graphene photonics and optoelectronics. Nat. Photon. **4**, 611 (2010).

[3] S. Z. Butler, S. M. Hollen, L. Cao, Y. Cui, J. A. Gupta, H. R. Gutierrez, T. F. Heinz, S. S. Hong, J. Huang, A. F. Ismach, E. J.-Halperin, M. Kuno, V. V. Plashnitsa, R. D. Robinson, R. S. Ruoff, S. Salahuddin, J. Shan, L. Shi, M. G. Spencer, M. Terrones, W. Windl, and J. E. Goldberger, Progress, challenges, and opportunities in two-dimensional materials beyond graphene. ACS Nano 7, 2898 (2013).

[4] Q. H. Wang, K. Kalantar-Zadeh, A. Kis, J. N. Coleman, M. S. Strano, Electronics and optoelectronics of two dimensional transition metal dichalcogenides. Nat. Nanotechnol. **7**, 699 (2012).

[5] W. Xin, X.-K. Li, X.-L. He, B.-W. Su, X.-Q. Jiang, K.-X. Huang, X.-F. Zhou, Z.-B. Liu, and J.-G. Tian, Black-Phosphorus-Based Orientation-Induced Diodes, Adv. Mater. **30**, 1704653 (2017)

[6] K. F. Mak, C. Lee, J. Hone, J. Shan, and T. F. Heinz, Atomically Thin MoS_2: A New Direct-Gap Semiconductor, Phys. Rev. Lett. **105**, 136805 (2010).

[7] M. Amani, D.-H. Lien, D. Kiriya, J. Xiao, A. Azcatl, J. Noh, S. R. Madhvapathy, R. Addou, S. KC, M. Dubey, K. Cho, R. M. Wallace, S.-C. Lee, J.-H. He, J. W. Ager III, X. Zhang, E. Yablonovitch, and A. Javey, Near-unity photoluminescence quantum yield in MoS_2, Science **350**, 1065 (2015)

[8] K. F. Mak and J. Shan, Photonics and optoelectronics of 2D semiconductor transition metal dichalcogenides, Nat. Photon. **10**, 216 (2016)

[9] S. Sampat, T. Guo, K. Zhang, J. A. Robinson, Y. Ghosh, K. P. Acharya, H. Htoon, J. A. Hollingsworth, Y. N. Gartstein, and A. V. Malko, Exciton and Trion Energy Transfer from Giant Semiconductor Nanocrystals to MoS_2 Monolayers. ACS Photonics **3**, 708 (2016).

[10] J. S. Ross, S. Wu, H. Yu, N. J. Ghimire, A. M. Jones, G. Aivazian, J. Yan, D. G. Mandrus, D. Xiao, W. Yao, and X. Xu, Electrical control of neutral and charged excitons in a monolayer semiconductor. Nat. Commun. **4**, 1474 (2013).

[11] K. F. Mak, D. Xiao, and J. Shan, Light–valley interactions in 2D semiconductors, Nat. Photon. 12, 451 (2018)

[12] M.-L. Tsai, S.-H. Su, J.-K. Chang, D.-S. Tsai, C.-H. Chen, C.-I Wu, L.-J. Li, L.-J. Chen, and J.H. He Monolayer MoS_2 Heterojunction Solar Cells. ACS nano, **8**, 8317 (2014)

[13] E. Singh, K. S. Kim, G. Y. Yeom, and H. S. Nalwa, Atomically Thin-Layered Molybdenum Disulfide (MoS_2) for Bulk-Heterojunction Solar Cells, ACS Appl. Mater. Interfaces, **9**, 3223 (2017)

[14] L. Yuan, T. Wang, T. Zhu, M. Zhou, and L. Huang, Exciton Dynamics, Transport, and Annihilation in Atomically Thin Two-Dimensional Semiconductors, J. Phys. Chem. Lett. **8**, 3371 (2017)
[15] Y. Tamai, H. Ohkita, H. Benten, and S. Ito, Exciton diffusion in conjugated polymers: from fundamental understanding to improvement in photovoltaic conversion efficiency. J. phys. Chem. Lett. **6**, 3417 (2015).
[16] M. S. Matthew, W. A. Luhman, and R. J. Holmes. Tailored exciton diffusion in organic photovoltaic cells for enhanced power conversion efficiency. Nature Mater. **12**, 152 (2013).
[17] J. D. A. Lin, O. V. Mikhnenko, J. Chen, Z. Masri, A. Ruseckas, A. Mikhailovsky, R. P. Raab, J. Liu, P. W. M. Blom, M. A. Loi, C. J. Garcia-Cervera, I. D. W. Samuel, and T.-Q. Nguyen, Systematic study of exciton diffusion length in organic semiconductors by six experimental methods. Mater. Horiz. **1**, 280 (2014).
[18] Y. Yu, Y. Yu, C. Xu, A. Barrette, K. Gundogdu, and L. Cao, Fundamental limits of exciton-exciton annihilation for light emission in transition metal dichalcogenide monolayers, Phys. Rev. B **93**, 201111(R) (2016)
[19] T. Kato and T. Kaneko, Transport Dynamics of Neutral Excitons and Trions in Monolayer WS_2, ACS Nano **10**, 9867 (2016)
[20] M. Palummo, M. Bernardi, and J. C. Grossman, Exciton Radiative Lifetimes in Two-Dimensional Transition Metal Dichalcogenides, Nano Lett. **15**, 2794 (2015)
[21] F. Wu, F. Qu, and A. H. MacDonald, Exciton band structure of monolayer MoS_2, Phys. Rev. B **91**, 075310 (2015)
[22] J. B. Pendry, Negative Refraction Makes a Perfect Lens. Phys. Rev. Lett., **85**, 3966 (2000).
[23] R. Maas, J. Parsons, N. Engheta, and A. Polman, Experimental realization of an epsilon-near-zero metamaterial at visible wavelengths, Nat. Photon. **7**, 907, (2013)
[24] N. Yu and F. Capasso, Flat optics with designer metasurfaces, Nat. Mater. 13, 139 (2014)
[25] M. Esfandyarpour, E. C. Garnett, Y. Cui, M. D. McGehee, and M. L. Brongersma, Metamaterial mirrors in optoelectronic devices, Nat. Nanotechnol. **9**, 542 (2014).
[26] H. Choi, S.-J. Ko, Y. Choi, P. Joo, T. Kim, B. R. Lee, J.-W. Jung, H. J. Choi, M. Cha, J.-R. Jeong, I.-W. Hwang, M. H. Song, B.-S. Kim, and J. Y. Kim, Versatile surface plasmon resonance of carbon-dot-supported silver nanoparticles in polymer optoelectronic devices, Nat. Photon. **7**, 732 (2013)
[27] H. Hodaei, A. U. Hassan, S. Wittek, H. Garcia-Gracia, R. El-Ganainy, D. N. Christodoulides, M. Khajavikhan, Enhanced sensitivity at higher-order exceptional points, Nature, 548, 187 (2017)
[28] J. B. Khurgin and G. Sun, Comparative analysis of spasers, vertical-cavity surface-emitting lasers and surface-plasmon-emitting diodes, Nat. Photon. **8**, 468 (2014)
[29] R. Zhang, Y. Zhang, Z. C. Dong, S. Jiang, C. Zhang, L. G. Chen, L. Zhang, Y. Liao, J. Aizpurua, Y. Luo, J. L. Yang, and J. G. Hou, Chemical mapping of a single molecule by plasmon-enhanced Raman scattering, Nature **498**, 82 (2013)
[30] H. N. S. Krishnamoorthy, Z. Jacob, E. Narimanov, I. Kretzschmar, and V. M. Menon, Topological Transitions in Metamaterials, Science **336**, 205 (2012)
[31] A. Poddubny, I. Iorsh, P. Belov, and Y. Kivshar, Hyperbolic metamaterials, Nat. Photon. **7**, 958-967 (2013)
[32] D. Lu, J. J. Kan, E. E. Fullerton, and Z. Liu, Enhancing spontaneous emission rates of molecules using nanopatterned multilayer hyperbolic metamaterials, Nat. Nanotechnol. **9**, 48-53 (2014)
[33] T. Tumkur, G. Zhu, P. Black, Y. A. Barnakov, C. E. Bonner, and M. A. Noginov, Control of spontaneous emission in a volume of functionalized hyperbolic metamaterial, Appl. Phys. Lett. **99**, 151115 (2011)
[34] K. J. Lee, Y. U. Lee, S. J. Kim, and P. André, Hyperbolic dispersion dominant regime identified through spontaneous emission variations near metamaterial interfaces, Adv. Mater. Interfaces **5**, 1701629 (2018)
[35] K. J. Lee, Y. Xiao, J. H. Woo, E. Kim, D. Kreher, A.-J. Attias, F. Mathevet, J.-C. Ribierre, J. W. Wu, and P. André. Charge-transfer dynamics and nonlocal dielectric permittivity tuned with metamaterial structures as solvent analogues, Nat. Mater. **16**, 722 (2017)

[36] K. J. Lee, Y. U. Lee, F. Fages, J.-C. Ribierre, J. W. Wu, and A. D'Aléo, Blue-Shifting intramolecular charge transfer emission by nonlocal effect of hyperbolic metamaterials, Nano Lett. **18**, 1476-1482 (2018)
[37] S. H. Aleithan, M. Y. Livshits, S. Khadka, Jeffrey J. Rack, M. E. Kordesch, and E. Stinaff, Broadband femtosecond transient absorption spectroscopy for a CVD MoS_2 monolayer, Phys. Rev. B **94**, 035445 (2016).
[38] A. Carvalho, R. M. Ribeiro, and A. H. Castro Neto, Band nesting and the optical response of two-dimensional semiconducting transition metal dichalcogenides, Phys. Rev. B **88**, 115205, (2013)
[39] D. Kozawa, R. Kumar, A. Carvalho, K. K. Amara, W. Zhao, S. Wang, M. Toh, R. M. Ribeiro, A. H. Castro Neto, K. Matsuda, and G. Eda. Photocarrier relaxation pathway in two-dimensional semiconducting transition metal dichalcogenides, Nat. Commun. **5**, 4543, (2014)
[40] L. Wang, Z. Wang, H.-Y. Wang, G. Grinblat, Y.-L. Huang, D. Wang, X.-H. Ye, X.-B. Li, Q. Bao, A.-S. Wee, S. A Maier, Q.-D. Chen, M.-L. Zhong, C.-W. Qiu, and H.-B. Sun, Slow cooling and efficient extraction of C-exciton hotcarriers in MoS_2 monolayer, Nat. Commun. **8**, 13906 (2016)
[41] W. Li, A. G. Birdwell, M. Amani, R. A. Burke, X. Ling, Y.-H. Lee, X. Liang, L. Peng, C. A. Richter, J. Kong, D. J. Gundlach, and N. V. Nguyen, Broadband optical properties of large-area monolayer CVD molybdenum disulfide, Phys. Rev. B **90**, 195434 (2014)
[42] D. Sun, Y. Rao, G. A. Reider, G. Chen, Y. You, L. Brézin, A. R. Harutyunyan, and T. F. Heinz, Observation of Rapid Exciton−Exciton Annihilation in Monolayer Molybdenum Disulfide, Nano Lett. **14**, 5625 (2014).
[43] N. Kumar, Q. Cui, F. Ceballos, D. He, Y. Wang, and H. Zhao, Exciton-exciton annihilation in $MoSe_2$ monolayers, Phys. Rev. B **89**, 125427 (2014)
[44] L. Yuan and L. Huang, Exciton dynamics and annihilation in WS_2 2D semiconductors, Nanoscale **7**, 7402, (2015)
[45] A. Ghazaryan, M. Hafezi, and P. Ghaemi, Anisotropic exciton transport in transition-metal dichalcogenides, Phys. Rev. B **97**, 245411 (2018)
[46] C. L. Cortes and Z. Jacob, Fundamental figures of merit for engineering Förster resonance energy transfer, Opt. Express **26**, 19371 (2018)
[47] Supplementary Material
[48] E. Engel, K. Leo, and M. Hoffmann, Ultrafast relaxation and exciton–exciton annihilation in PTCDA thin films at high excitation densities, Chem. Phys. **325**, 170–177 (2006).
[49] H.-Y. Shin, J. H. Woo, M. J. Gwon, M. Barthelemy, M. Vomir, T. Muto, K. Takaishi, M. Uchiyama, D. Hashizume, T. Aoyama, D.-W. Kim, S. Yoon, J.-Y. Bigot, J. W. Wu, J. C. Ribierre. Exciton diffusion in near-infrared absorbing solution-processed organic thin films, Phys. Chem. Chem. Phys. **15**, 2867 (2013)
[50] M. Lunz, A. L. Bradley, V. A. Gerard, S. J. Byrne, Y. K. Gun'ko, V. Lesnyak, and N. Gaponik, Concentration dependence of Förster resonant energy transfer between donor and acceptor nanocrystal quantum dot layers: Effect of donor-donor interactions, Phys. Rev. B 83, 115423 (2011)